Supplementary Information for

Inducing Preferential Intercalation of Zn^{2+} in MnO_2 with Abundant Oxygen Defects for High-Performance Aqueous Zinc-Ion Battery

Simin Dai[a]†, Xinyan Zhuang[a]†, Hongrun Jin[a]†, Ruixuan Yang[b], Yan Wang[a], Bei Qi[a], Wenhuan Guo[a], Kefeng Xie[c], Zhimi Hu [a], Meilin Liu[d] and Liang Huang[a]*

[a] Wuhan National Laboratory for Optoelectronics, School of Optical and Electronic Information, Huazhong University of Science and Technology, Wuhan, 430074, China

[b] School of Materials Science and Engineering, Xi'an University of Technology, Xi'an 710048, China

[c] School of Chemistry and Chemical Engineering, Lanzhou Jiaotong University, Lanzhou, 730000, China

[d] School of Materials Science and Engineering, Georgia Institute of Technology, 771 Ferst Drive, Atlanta, Georgia 30332-0245, United States

†These authors contribute equally to this work

*Corresponding authors' e-mail addresses: huangliang421@hust.edu.cn

Experimental Section

Preparation of MnO_2 and Oxygen-Deficient MnO_2 Nanosheets

In a typical synthesis procedure, 5 g of potassium nitrate (KNO_3) powder was added into a quartz crucible and transferred into the muffle furnace at a temperature of 380 °C in the air atmosphere. Once the KNO_3 powder turns into the molten state after heating for 10 min, 0.2 g of manganese sulfate ($MnSO_4$) powder was added for a short reaction time of 1 min. Then, the product was removed from the muffle furnace and quenched to room temperature under ambient conditions. Finally, the product was washed with deionized (DI) water to remove excess KNO_3 and dried in an oven at 60 °C to obtain MnO_2 nanosheets. To further prepare oxygen-deficient MnO_2 (O_d-MnO_2) nanosheets, the MnO_2 nanosheets obtained above were homogeneously dispersed in 10 mL of hexane in a glass bottle. Then in the glove box, 2 mL of n-butyllithium solution (1.6 M in hexane, 15% solution) was added into the glass bottle and stirred on a magnetic stirrer for 24 h. Afterwards, ethanol was added to consume the n-butyllithium which was not fully reacted. Finally, the reaction product was washed with DI water and dried at 60 °C to obtain O_d-MnO_2 nanosheets. N-butyllithium has strong reducing properties, which can partially reduce Mn and generate Li_2O ($MnO_2+2xLiC_4H_9 = MnO_{2-x} + xLi_2O + xC_8H_{18}$), resulting in the formation of oxygen defects.

Preparation of MnO_2 and O_d-MnO_2 Self-Supporting Electrodes

O_d-MnO_2 nanosheets and carbon nanotube (CNT) powder were mixed in DI water with a mass ratio of 7:3, and a small amount of sodium dodecyl benzene sulfonate (SDBS) as surfactant was added. Then the mixture was ultrasonicated for 1 h for homogeneous dispersion. Afterwards, the dispersion was filtered with Celgard membrane as the filter membrane. Finally, the complete O_d-MnO_2 self-supporting electrode can be peeled off after the product was dried naturally overnight in a fume hood. The MnO_2 self-supporting electrode is prepared in the same way.

Material Characterizations

XRD measurements were taken on a powder diffractometer (X'Pert3 powder, PANalytical) at 40 kV accelerating voltage and 40 mA current with Cu Kα radiation (λ=1.5418 Å). The morphological structure was investigated using SEM (Nova 450 Nano, FEI) and TEM (Titan G2 60-300, 300 kV). The specific surface area was determined by nitrogen adsorption-desorption curves, which was conducted on the surface area analyzer (Micromeritics 3Flex Version 5.00) and estimated by BET

(Brunauer-Emmett-Teller) method. The chemical composition and valence state of the samples were characterized by XPS using Thermo Scientific K-Alpha with Al Kα X-ray source (hv=1486.6 eV). Raman spectra were conducted on LabRAM HR800 with an excitation wavelength of 532 nm. ICP-OES (Thermo Fisher iCAP PRO) was used to determine the mass fraction of Zn and Mn elements. The thickness of the electrode slice was determined by a step profiler (Millimar C1208).

Electrochemical Measurements

The electrochemical performances of the batteries were evaluated using CR2025 coin-type cells on electrochemical workstation (EC-lab) and LAND battery testing system (M340A, LANHE) at a constant temperature of 25 ℃. The MnO_2 and O_d-MnO_2 self-supporting electrode with mass loading of around 2 mg cm^{-2}, the Zn foil with a diameter of 15 mm and thickness of 20 μm, the glass fiber with a diameter of 19 mm and 2 M Zn $(CF_3SO_3)_2$ + 0.1 M $MnSO_4$ solution were used as the cathode, anode, separator, and electrolyte, respectively. All the electrochemical tests in this paper were done in a two-electrode configuration. CV and GCD were carried out within a potential range from 0.8 V to 1.9 V versus Zn^{2+}/Zn. EIS spectra were recorded over the frequency ranging from 500 kHz to 10 mHz with an amplitude of 10 mV. Specific capacity, energy density, and power density were calculated based on the mass of the active materials from the cathode.

GITT was conducted to calculate the ion diffusion coefficient (D_{ion}) by the following equation:[1]

$$D = \frac{4L^2}{\pi\tau}\left(\frac{\Delta E_s}{\Delta E_t}\right)^2 \quad (1)$$

where τ is the constant current pulse time (s), ΔE_s is the steady-state potential change (V) caused by the current pulse, and ΔE_t is the potential change (V) during the constant current pulse after eliminating the iR drop. L is ion diffusion length, which is approximate to the thickness of electrode (cm) for compact electrode. In our GITT test, the cycle containing a 10 min galvanostatic charge/discharge pulse at 0.1 A g^{-1} and a 30 min open circuit relaxation step, was repeated until the discharge voltage reaching 0.8 V (the value is 1.9 V during charge process).

Calculation method of the specific capacity contribution percentage of Zn^{2+} intercalation

The specific capacity contributed by Zn^{2+} is roughly calculated based on the

atomic fraction of zinc, and then the specific capacity contribution percentage of Zn^{2+} intercalation is calculated based on the measured total specific capacity (denoted as *c*). Specifically, according to the equation $xZn^{2+} + 2xe^- + MnO_2 \rightarrow MnOOZn_x$, the atomic fraction of Zn (denoted as *a*), and the atomic fraction of Mn (denoted as *b*), the chemical formula of the discharge product can be known as Mn_bOOZn_a ($MnOOZn_{a/b}$). When *y* mol MnO_2 is involved in the reaction, the number of transferred electrons is $2ay/b$ mol. It is known that 1 mol $e^- \approx 26800$mAh, so the capacity contribution of Zn^{2+} is $53600ay/b$ mAh, and the specific capacity contribution of Zn^{2+} is $\frac{53600ay/b}{87 * y} = 616a/b$ mAh g^{-1}, where 87 is the relative atomic mass of MnO_2.Therfore, the specific capacity contribution percentage of Zn^{2+} intercalation is $616a/(bc)$ %.

Density functional theory (DFT) calculations

In this article, all DFT calculations were conducted using the Cambridge Sequential Total Energy Package (CASTEP) module within the Materials Studio software package. The interactions between electrons were described using the Perdew–Burke–Ernzerhof (PBE) interaction correlation functional in the generalized gradient approximation (GGA). The energy cutoff of the plane wave basis was set to 500 eV. The Gamma center used a MonkHorst-Pack 3 × 3 × 3 k-point grid to sample the First Brillouin-zone, and optimized the geometric structure. The convergence criteria for geometry optimization were 10^{-5} eV per atom for energy, 0.1 eV $Å^{-1}$ for force, 0.005 Å for displacement. The tolerance for self-consistent calculation (SCF) was set to 1×10^{-5} eV per atom. The adsorptihon energy (Eads) was calculated by

$$E_{ads} = E_{MnO_2 + H(Zn)} - E_{MnO_2} - E_{H(Zn)} \quad (2)$$

where $E_{MnO_2 + H(Zn)}$, E_{MnO_2}, $E_{H(Zn)}$ represent the energy of the H/Zn on MnO_2, MnO_2, and H/Zn atom, respectively.[2-3]

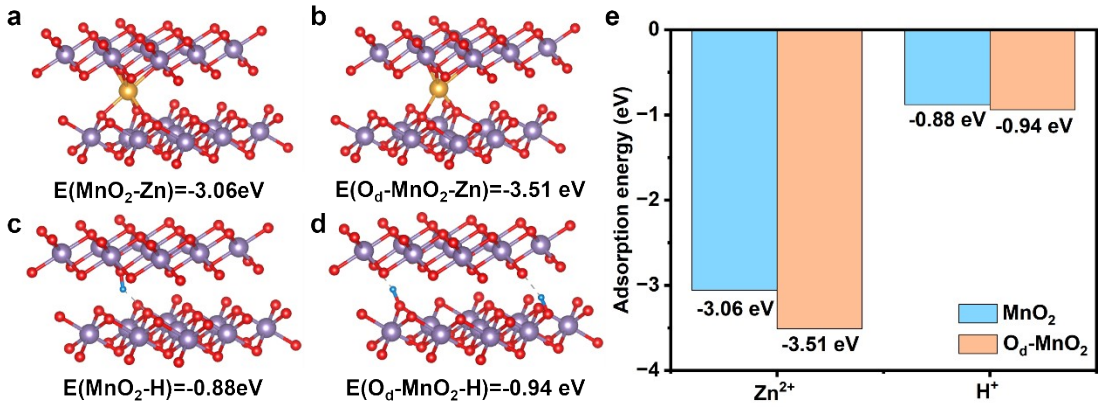

Fig. S1 The schematic illustration of Zn^{2+} adsorption energies for (a) pristine MnO_2 and (b) O_d-MnO_2. H^+ adsorption energies for (c) pristine MnO_2 and (d) O_d-MnO_2. (e) Comparison of the adsorption energies of Zn^{2+} and H^+ on pristine MnO_2 and O_d-MnO_2.

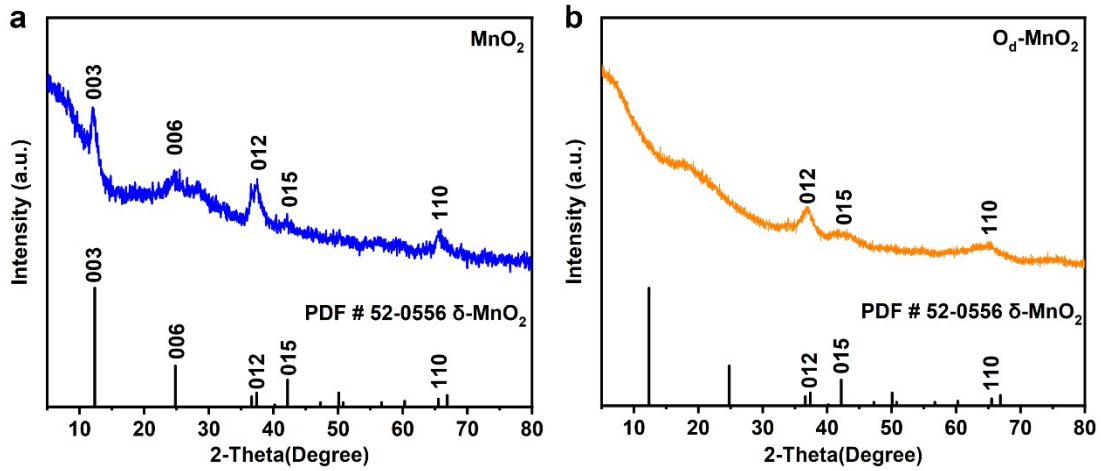

Fig. S2 The XRD patterns of (a) pristine MnO_2 and (b) O_d-MnO_2.

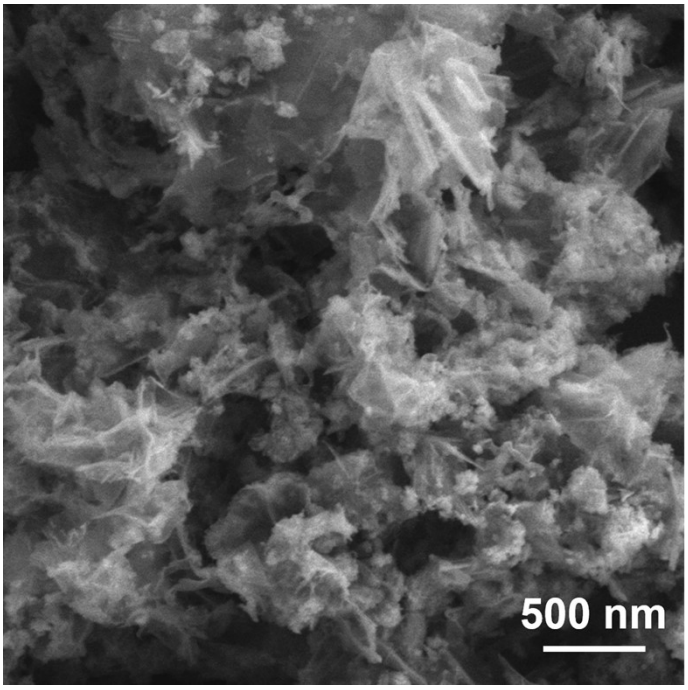

Fig. S3 The SEM image of pristine MnO_2.

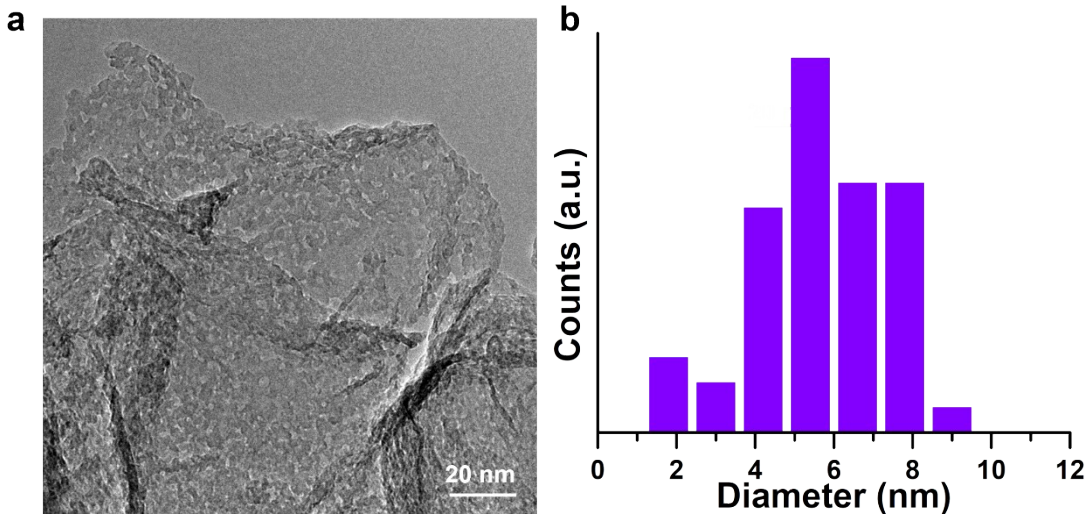

Fig. S4 (a) The TEM image of O_d-MnO_2, and (b) the corresponding pore diameter distribution according to (a).

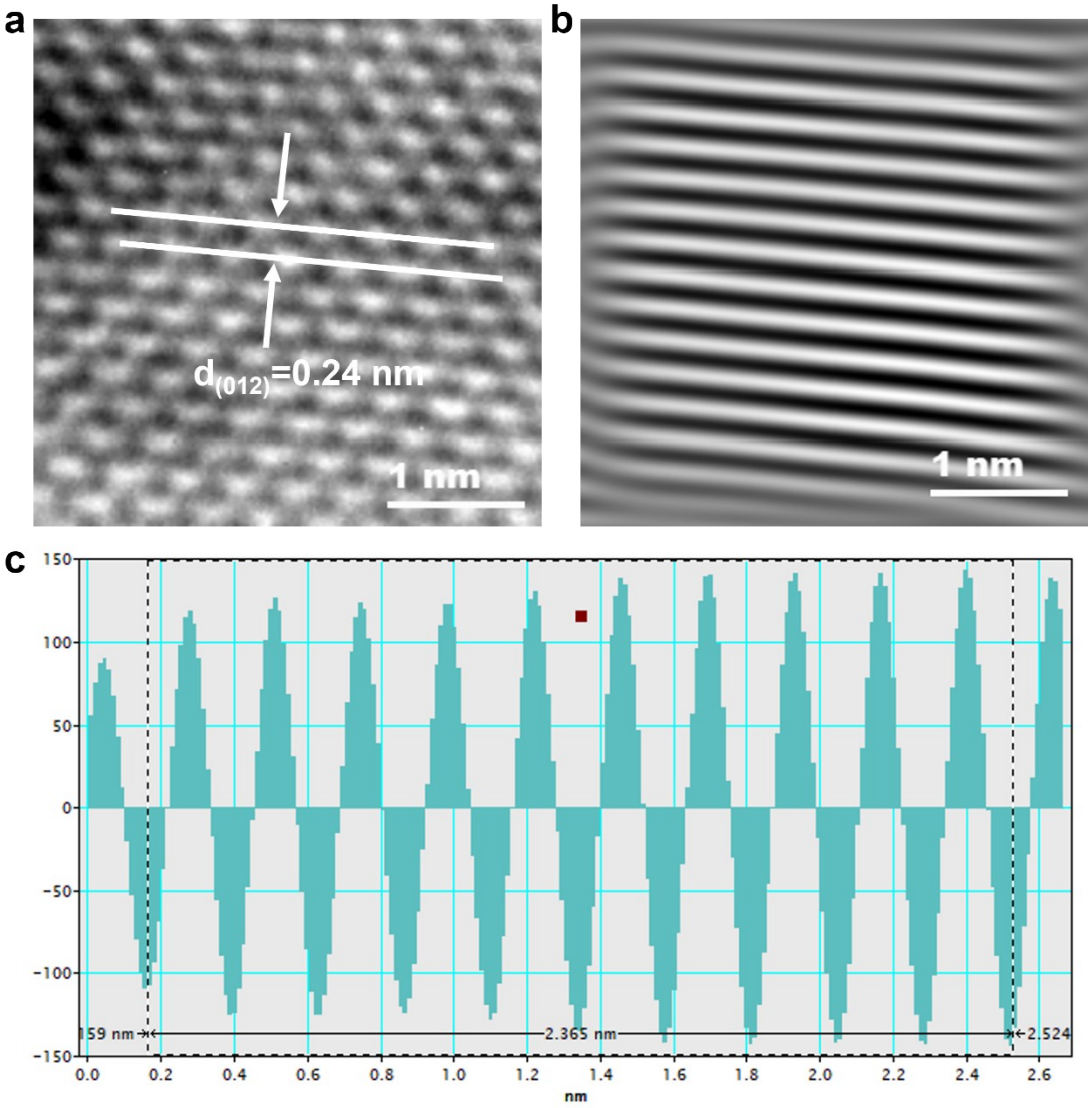

Fig. S5 The high-resolution transmission electron microscopy (HRTEM) analysis of O_d-MnO_2. (a) The HRTEM magnification image. (b) The inverse FFT patterns and (c) normalized intensity variations in (a).

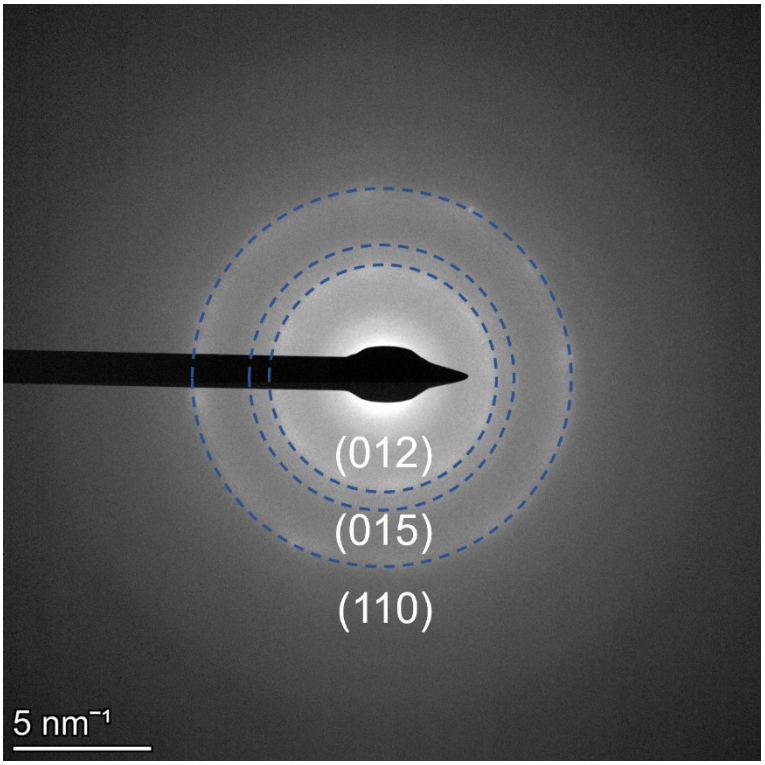

Fig. S6 The selected area electron diffraction (SAED) pattern of O_d-MnO_2.

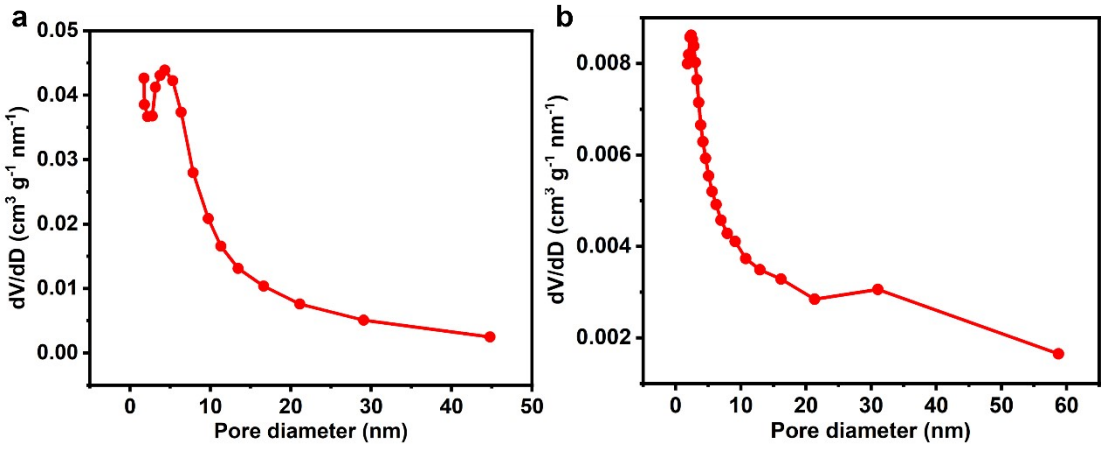

Fig. S7 The pore size distribution plots of (a) O_d-MnO_2 and (b) MnO_2 corresponding to nitrogen adsorption-desorption isotherms in Fig. 2e.

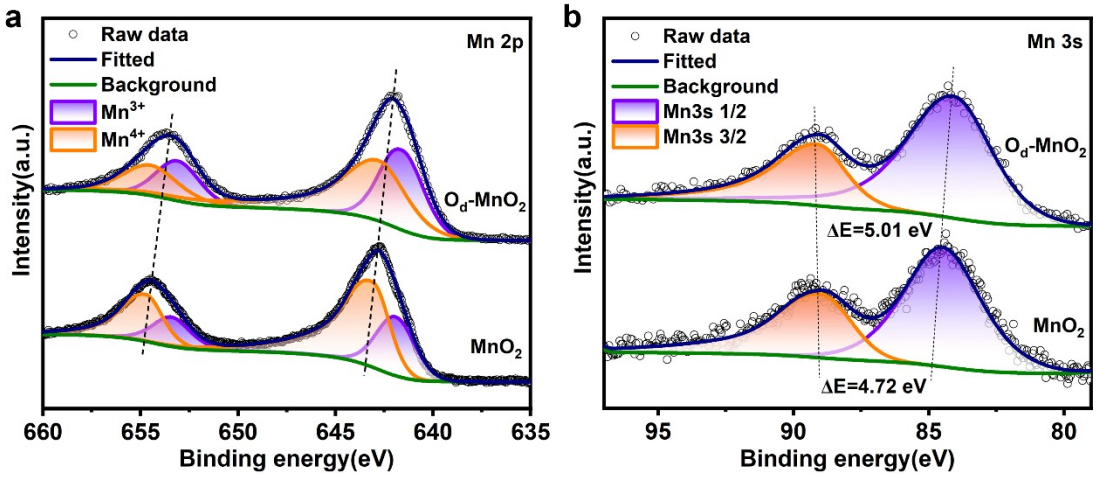

Fig. S8 (a) Mn 2p high resolution XPS spectra. (b) Mn 3s high resolution XPS spectra of MnO_2 and O_d-MnO_2.

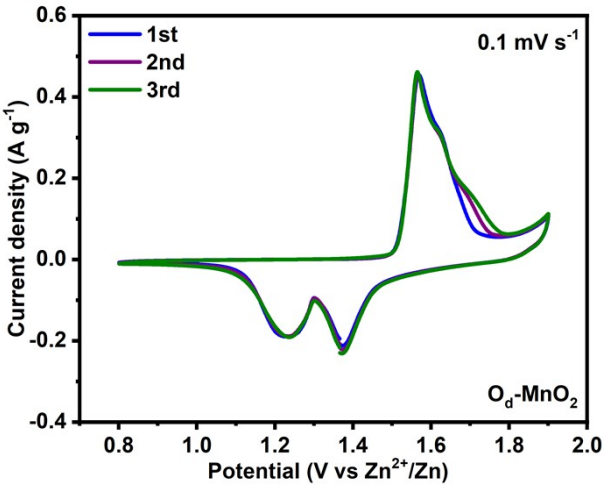

Figure S9. The initial three cycles of CV curves of O_d-MnO_2 electrode.

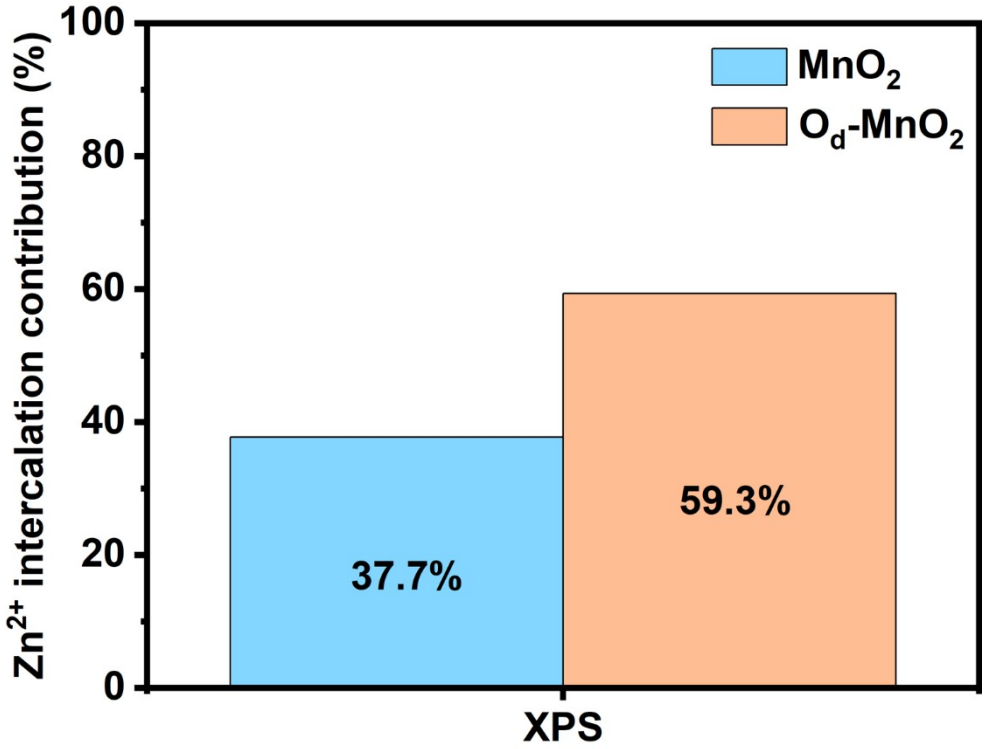

Fig. S10. The percentage of Zn^{2+} intercalation contribution calculated by XPS tests.

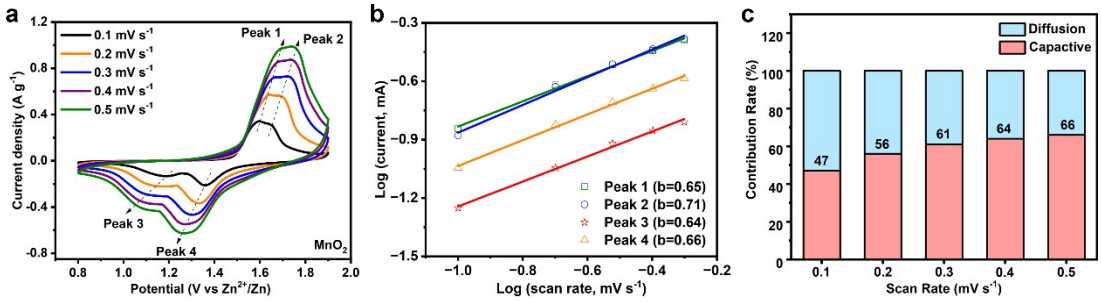

Fig. S11 (a) The CV curves of Zn/MnO_2 battery at different scan rates. (b) Determination of the b value using the relationship between peak current and scan rate. (c) the corresponding percent of pseudocapacitive contribution.

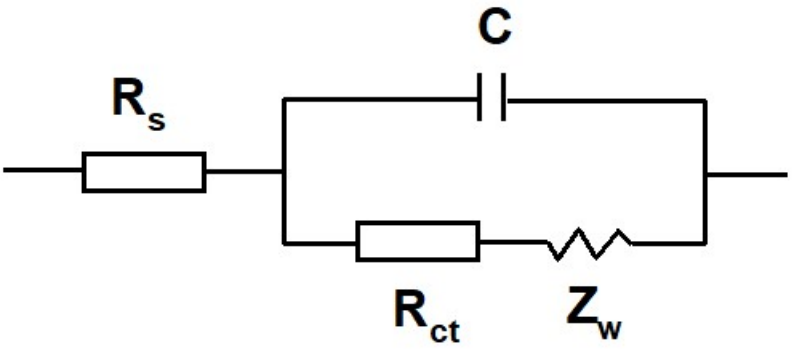

Figure S12. The equivalent circuit model.

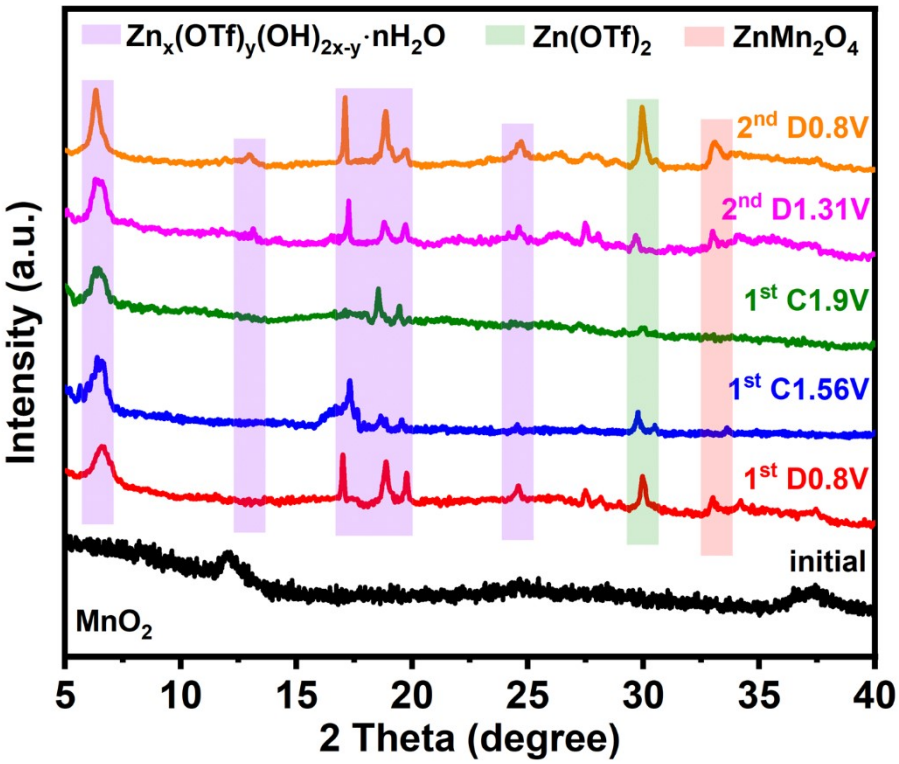

Fig. S13 The ex-situ XRD pattern of Zn/MnO_2 battery at different states.

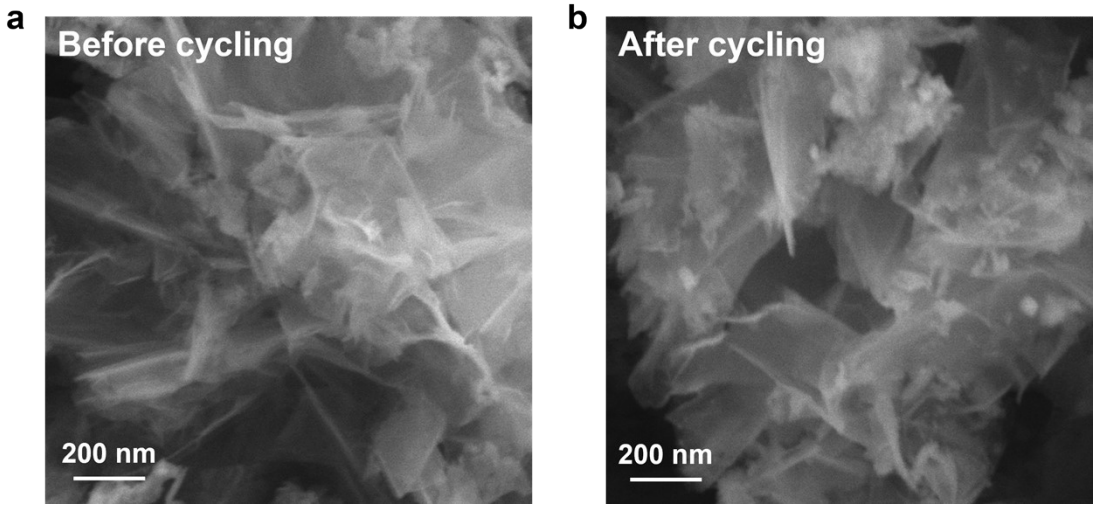

Fig. S14 The SEM images of O_d-MnO_2 electrodes (a) before and (b) after cycling.

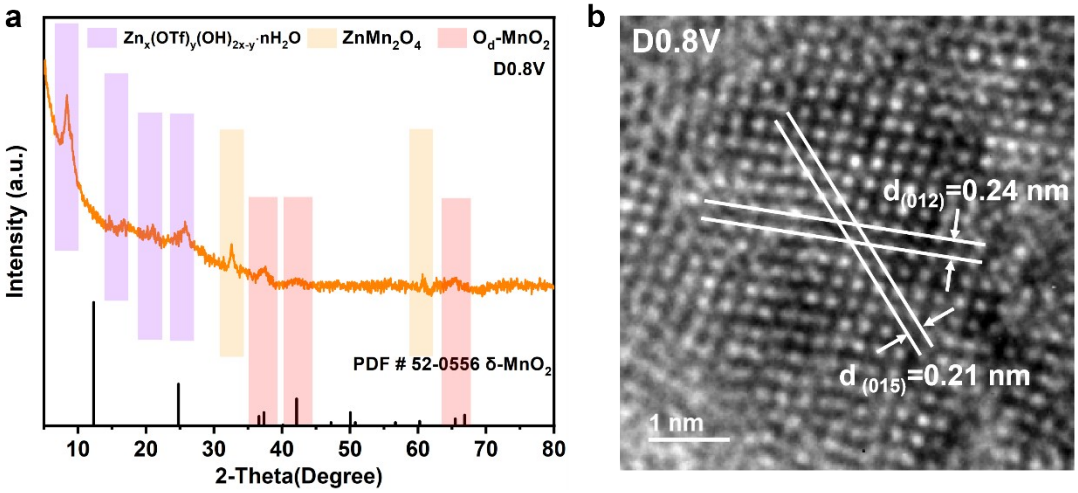

Fig. S15 (a) The XRD pattern and (b) HRTEM images of the O_d-MnO_2 electrode at fully discharged state.

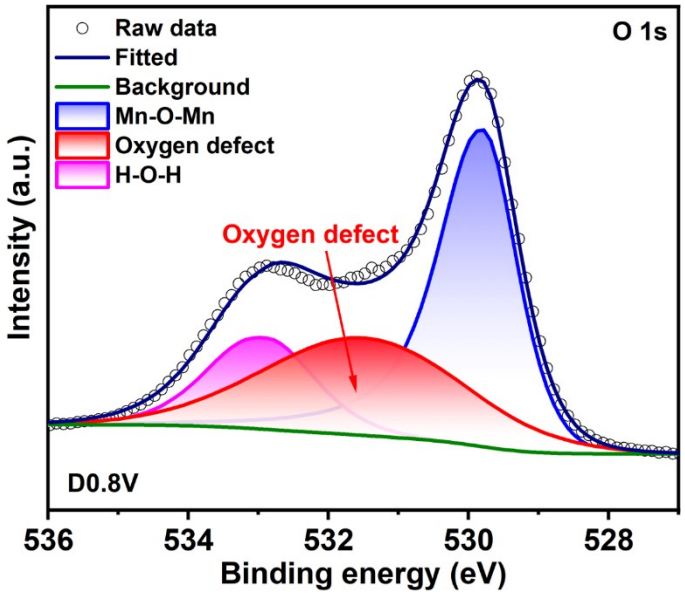

Fig. S16 The high-resolution O 1s spectra of the O_d-MnO_2 electrode at fully discharged state.

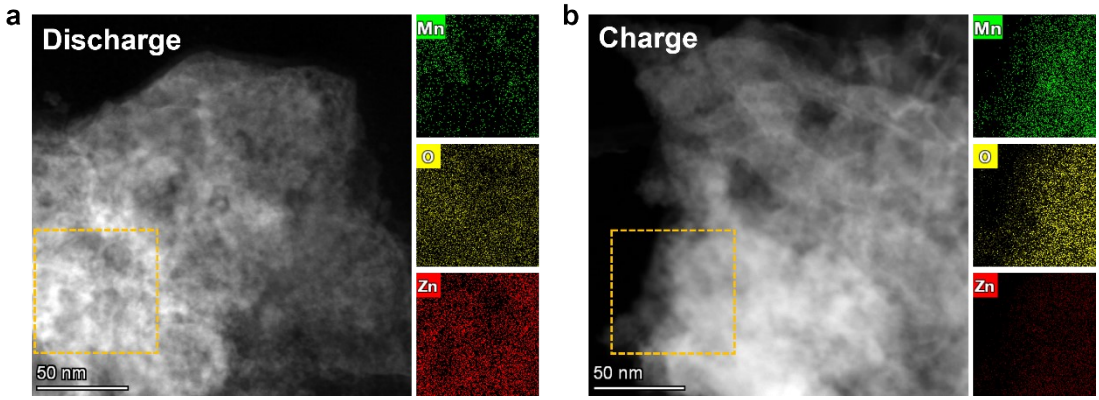

Fig. S17 The element mapping images of the O_d-MnO_2 electrode at (a) fully discharged state and (b) fully charged state.

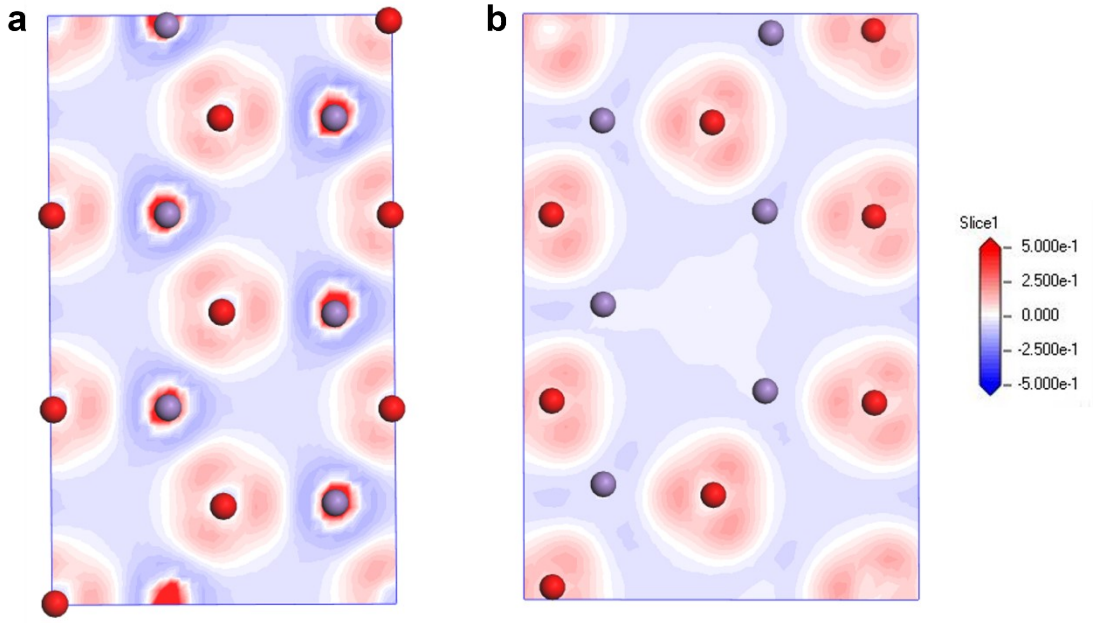

Fig. S18 The charge density distribution of (a) pristine MnO_2 and (b) O_d-MnO_2.

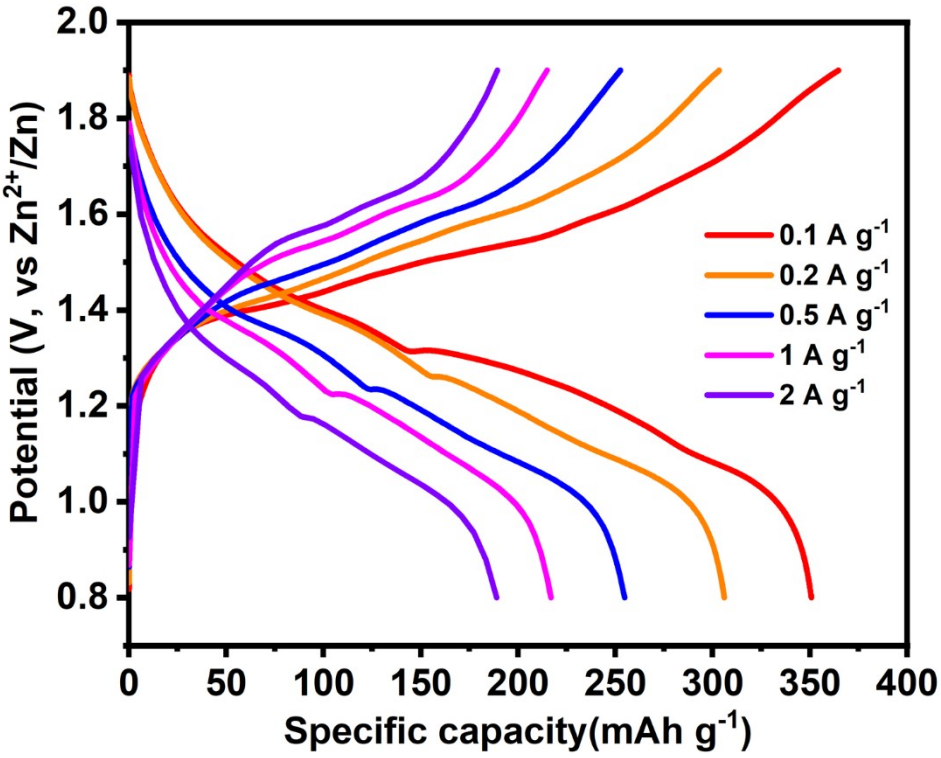

Fig. S19 The representative galvanostatic charge/discharge curves at different current densities of O_d-MnO_2.

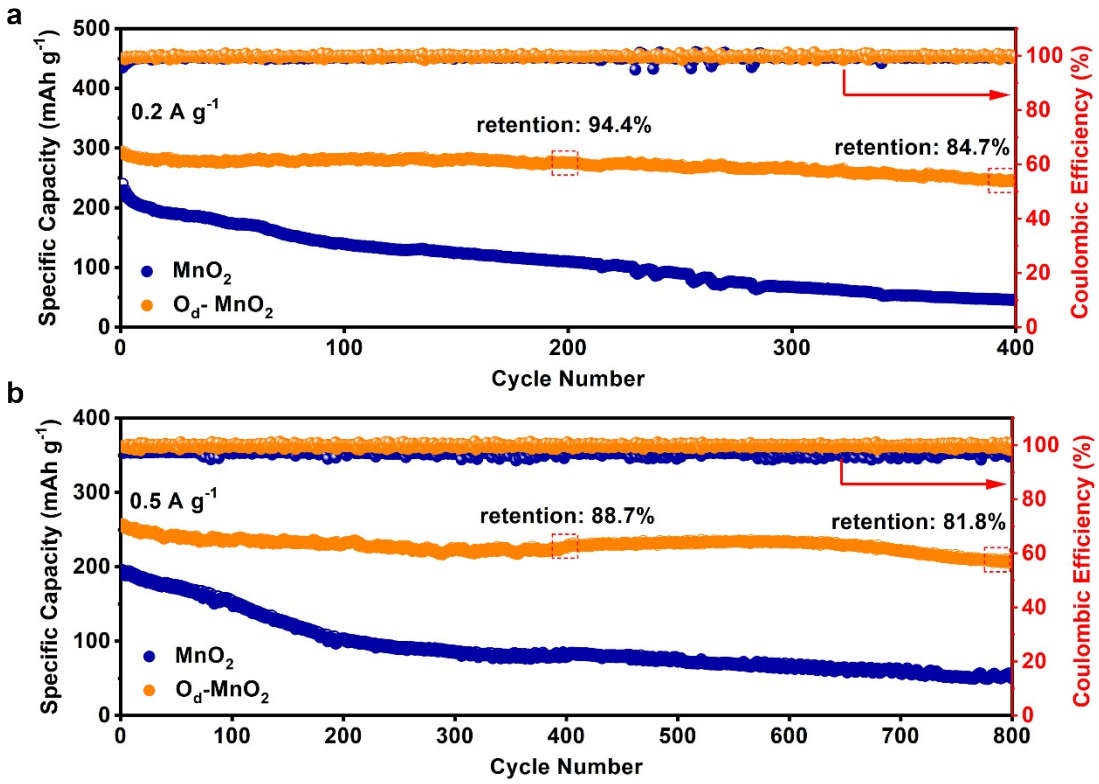

Fig. S20 The long-life cycling performance of Zn/MnO_2 and Zn/O_d-MnO_2 coin cells at current densities of (a) 0.2 A g^{-1} and (b) 0.5 A g^{-1}.

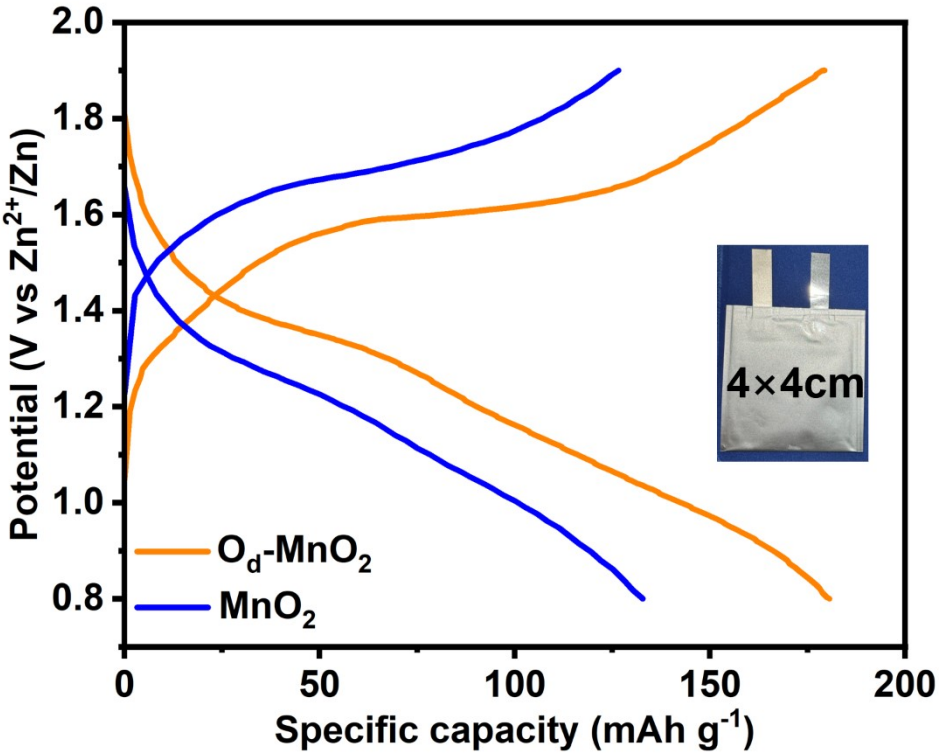

Fig. S21 The charge-discharge curves of Zn/MnO_2 and Zn/O_d-MnO_2 pouch cells at a rate of 1C.

Table S1. The mass fraction of Mn and Zn elements of the fully discharged MnO_2 and O_d-MnO_2 of ICP results.

Sample	Tested element	Mass fraction(%)
O_d-MnO_2	Mn	14.4
	Zn	4.81
MnO_2	Mn	15.1
	Zn	3.22

Table S2. The atomic fraction of Mn and Zn elements of the fully discharged MnO_2 and O_d-MnO_2 of XPS results.

Sample	Tested element	Atomic fraction(%)
O_d-MnO_2	Mn	27.33
	Zn	8.09
MnO_2	Mn	28.62
	Zn	5.38

Reference

1 G. Fang, C. Zhu, M. Chen, J. Zhou, B. Tang, X. Cao, X. Zheng, A. Pan, S. Liang, *Adv. Funct. Mater.*, 2019, **29**, 1808375.

2 T. Xiong, Z. G. Yu, H. Wu, Y. Du, Q. Xie, J. Chen, Y.-W. Zhang, S. J. Pennycook, W. S. V. Lee, J. Xue, *Adv. Energy Mater*, 2019, **9**, 1803815.

3 Y. Li, X. Li, H. Duan, S. Xie, R. Dai, J. Rong, F. Kang, L. Dong, *Chem. Eng. J.*, 2022, **441**, 136008.